Inorg. Chem. **2004**, *43*, 6177−6187

Binding of DNA Purine Sites to Dirhodium Compounds Probed by Mass Spectrometry

Helen T. Chifotides,[†] John M. Koomen,[‡] Mijeong Kang,[†] Shane E. Tichy,[‡] Kim R. Dunbar,*[,†] and David H. Russell*[,‡]

Chemistry Department and Laboratory for Biological Mass Spectrometry, Texas A&M University, College Station, Texas 77843

Received March 19, 2004

The adducts formed between the antitumor active compounds $[Rh_2(O_2CCH_3)_2(CH_3CN)_6](BF_4)_2$, $Rh_2(O_2CCH_3)_4$, and $Rh_2(O_2CCF_3)_4$ with DNA oligonucleotides have been assessed by matrix-assisted laser desorption ionization (MALDI) and nanoelectrospray (nanoESI) coupled to time-of-flight mass spectrometry (TOF MS). A series of MALDI studies performed on dipurine (**AA**, **AG**, **GA**, and **GG**)-containing single-stranded oligonucleotides of different lengths (tetra- to dodecamers) led to the establishment of the relative reactivity *cis*-$[Pt(NH_3)_2(OH_2)_2]^{2+}$ (activated cisplatin) ≈ $Rh_2(O_2CCF_3)_4$ > *cis*-$[Pt(NH_3)_2Cl_2]$ (cisplatin) ≫ $[Rh_2(O_2CCH_3)_2(CH_3CN)_6](BF_4)_2$ > $Rh_2(O_2CCH_3)_4$ ≈ $Pt(C_6H_6O_4)(NH_3)_2$ (carboplatin). The relative reactivity of the complexes is associated with the lability of the leaving groups. The general trend is that an increase in the length of the oligonucleotide leads to enhanced reactivity for $Rh_2(O_2CCH_3)_2(CH_3CN)_6](BF_4)_2$ and $Rh_2(O_2CCH_3)_4$ (except for the case of $[Rh_2(O_2CCH_3)_2(CH_3CN)_6]^{2+}$, which reacts faster with the **GG** octamers than with the dodecamers), whereas the reactivity of $Rh_2(O_2CCF_3)_4$ is independent of the oligonucleotide length. When monitored by ESI, the dodecamers containing **GG** react faster than the respective **AA** oligonucleotides in reactions with $Rh_2(O_2CCF_3)_4$ and $Rh_2(O_2CCH_3)_2(CH_3CN)_6](BF_4)_2$, whereas **AA** oligonucleotides react faster with $Rh_2(O_2CCH_3)_4$. The mixed (**AG**, **GA**) purine sequences exhibit comparable rates of reactivity with the homopurine (**AA**, **GG**) dodecamers in reactions with $Rh_2(O_2CCH_3)_4$. The observation of initial dirhodium–DNA adducts with weak axial (*ax*) interactions, followed by rearrangement to more stable equatorial (*eq*) adducts, was achieved by electrospray ionization; the Rh–Rh bond as well as coordinated acetate or acetonitrile ligands remain intact in these dirhodium–DNA adducts. MALDI in-source decay (ISD), collision-induced dissociation (CID) MS−MS, and enzymatic digestion studies followed by MALDI and ESI MS reveal that, in the dirhodium compounds studied, the purine sites of the DNA oligonucleotides interact with the dirhodium core. Ultimately, both MALDI and ESI MS proved to be complementary, valuable tools for probing the identity and stability of dinuclear metal–DNA adducts.

Introduction

Interactions between metal ions and DNA are key cellular events in the mode of action of chemotherapeutic agents. Although the exact mechanism of activity of the potent anticancer agent cisplatin (*cis*-$[Pt(NH_3)_2Cl_2$ or *cis*-DDP) is not entirely understood, it is known that the replication and transcription events are inhibited upon cisplatin binding to DNA.[1−4] In particular, the formation of bifunctional intrastrand covalent cross links involving **GG** sites leads to bending and unwinding of the DNA duplex; furthermore, the presence of intrastrand cisplatin−DNA lesions enhances binding of high-mobility-group (HMG) domain proteins that are postulated to mediate the antitumor properties of the drug.[1,4,5]

* Authors to whom correspondence should be addressed. E-mail: dunbar@mail.chem.tamu.edu. Tel: (979) 845-5235. Fax: (979) 845-7177 (K.R.D.). E-mail: russell@mail.chem.tamu.edu. Tel: (979) 845-3345. Fax: (979) 845-9485 (D.H.R.).

[†] Chemistry Department.

[‡] Laboratory for Biological Mass Spectrometry.

(1) Huang, J.-C.; Zamble, D. B.; Reardon, J. T.; Lippard, S. J.; Sancar, A. *Proc. Natl. Acad. Sci. U.S.A.* **1994**, *91*, 10394−10398.

(2) Zhai, X.; Beckmann, H.; Jantzen, H.-M.; Essigmann, J. M. *Biochemistry* **1998**, *37*, 16307−16315.

(3) Ohndorf, U.-M.; Rould, M. A.; He, Q.; Pabo, C. O.; Lippard, S. J. *Nature* **1999**, *399*, 708−712.

(4) Lee, K.-B.; Wang, D.; Lippard, S. J.; Sharp, P. A. *Proc. Natl. Acad. Sci. U.S.A.* **2002**, *99*, 4239−4244.

10.1021/ic040040u CCC: $27.50
Published on Web 08/28/2004

The identification of metal−nucleic acid interactions is of fundamental importance to the understanding of the molecular basis of antitumor activity. Detailed structural information about the nature of these interactions requires a combination of chemical and biological techniques, as evidenced by the body of work reported for cisplatin. Structural characterization of crucial cisplatin−DNA adducts has been achieved by NMR spectroscopy and X-ray crystallography,[6,7] and although these techniques provide unambiguous and fine-structural details of the adducts, they require highly pure samples (crystalline samples for X-ray) in relatively large concentrations (mM for NMR).

Modern ionization methods, such as matrix-assisted laser desorption ionization (MALDI)[8] and electrospray ionization (ESI)[9] coupled to time-of-flight (TOF) mass spectrometry (MS) and tandem MS, are powerful analytical tools with the potential to complement other structural methods by rapidly delivering highly accurate information about the sequence and fragmentation of oligonucleotides[10−17] as well as metal−DNA interactions using very small quantities of the adducts (1 pmol or less).[18,19] The application of MS-based techniques for the characterization of metal−DNA complexes,[20,21] carcinogen−DNA adducts,[22] drug−DNA interactions,[19,23−25] and novel chemotherapeutic agents[26] has proven to be highly successful. Conversely, only a limited number of reports on the characterization of oligonucleotide complexes with metal ions other than platinum(II) are available.[21,27,28] Over the past decade, extensive MS characterization studies have been reported for cisplatin−DNA complexes. Claereboudt et al. employed laser microprobe (LAMMA) and fast atom bombardment (FAB) MS to characterize Pt adducts of DNA,[29,30] and Costello and Lippard applied FAB and MALDI techniques to probe cisplatin−DNA interactions.[31,32] The kinetics of the reaction between TTGGCCAA and $[Pt(NH_3)_3(OH_2)]^{2+}$ have been followed by MALDI,[33] and ESI MS has been used to examine the electrostatic association between $[Pt(NH_3)_4]^{2+}$ and DNA oligonucleotides.[34] The latter studies are particularly valuable because electrostatic interactions are proposed to be the first step in activated cisplatin−DNA binding.[34] Structural characterization by ESI MS−MS has also enabled researchers to identify key cisplatin binding sites to DNA.[35]

In past decades, an entirely different class of antitumor compounds, namely dinuclear carboxylate complexes of rhodium (Scheme 1, compounds **1**, **2**, and **3**), has attracted

Scheme 1. Schematic Structure of the Complexes $[Rh_2(O_2CCH_3)_2(CH_3CN)_6]^{2+}$ (**1**); $Rh_2(O_2CCH_3)_4$ (**2**); $Rh_2(O_2CCF_3)_4$ (**3**); *cis*-$[Pt(NH_3)_2Cl_2]$ (**4**); *cis*-$[Pt(NH_3)_2(H_2O)_2]^{2+}$ (**5**); $[Pt(C_6H_6O_4)(NH_3)_2]$ (**6**)

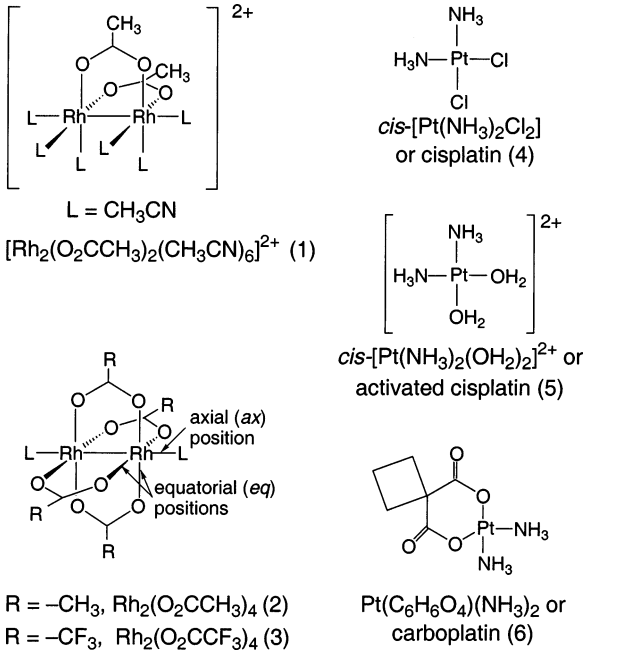

(5) Zlatanova, J.; Yaneva, J.; Leuba, S. H. *FASEB J.* **1998**, *12*, 791−799.
(6) Jamieson, E. R.; Lippard, S. J. *Chem. Rev.* **1999**, *99*, 2467−2498 and references therein.
(7) Lippert, B., Ed. *Cisplatin: Chemistry and Biochemistry of a Leading Anticancer Drug*; Wiley-VCH: Weinheim, Germany, 1999 and references therein.
(8) Karas, M.; Bachmann, D.; Bahr, U.; Hillenkamp, F. *Int. J. Mass Spectrom. Ion Processes* **1987**, *78*, 53−68.
(9) Yamashita, M.; Fenn, J. B. *J. Phys. Chem.* **1984**, *88*, 4451−4459.
(10) Zhu, L.; Parr, G. R.; Fitzgerald, M. C.; Nelson, C. M.; Smith, L. M. *J. Am. Chem. Soc.* **1995**, *117*, 6048−6056.
(11) Zhu, Y. F.; Taranenko, N. I.; Allman, S. L.; Taranenko, N. V.; Martin, S. A.; Haff, L. A.; Chen, C. H. *Rapid Commun. Mass Spectrom.* **1997**, *11*, 897−903.
(12) Wang, B. H.; Hopkins, C. E.; Belenky, A. B.; Cohen, A. S. *Int. J. Mass Spectrom. Ion Processes* **1997**, *169*, 331−350.
(13) Zhang, L.-K.; Gross, M. L. *J. Am. Soc. Mass Spectrom.* **2000**, *11*, 854−865.
(14) Krause, J.; Scalf, M.; Smith, L. M. *J. Am. Soc. Mass Spectrom.* **1999**, *10*, 423−429.
(15) Roskey, M. T.; Juhasz, P.; Smirnov, I. P.; Takach, E. J.; Martin, S. A. Haff, L. A. *Proc. Natl. Acad. Sci. U.S.A.* **1996**, *93*, 4724−4729.
(16) Little, D. P.; Chorush, R. A.; Speir, J. P.; Senko, M. W.; Kelleher, N. L.; McLafferty, F. W. *J. Am. Chem. Soc.* **1994**, *116*, 4893−4897.
(17) Ni, J.; Chan, K. *Rapid Commun. Mass Spectrom.* **2001**, *15*, 1600−1608.
(18) Berkenkamp, S.; Kirpekar, F.; Hillenkamp, F. *Science* **1998**, 281, 260−262.
(19) Wan, K. X.; Shibue, T.; Gross, M. L. *J. Am. Chem. Soc.* **2000**, *122*, 300−307.
(20) Hettich, R. L. *J. Am. Soc. Mass Spectrom.* **1999**, *10*, 941−949.
(21) Beck, J. L.; Humphries, A.; Sheil, M. M.; Ralph, S. F. *Eur. Mass Spectrom.* **1999**, *5*, 489−500 and references therein.
(22) Marzilli, L. A.; Wang, D.; Kobertz, W. R.; Essigmann, J. M.; Vouros, P. *J. Am. Soc. Mass Spectrom.* **1998**, *9*, 676−682.
(23) Harsch, A.; Marzilli, L. A.; Bunt, R. C.; Stubbe, J.; Vouros, P. *Nucleic Acids Res.* **2000**, *28*, 1978−1985.
(24) Gabelica, V.; De Pauw, E.; Rosu, F. *J. Mass Spectrom.* **1999**, *34*, 1328−1337.
(25) Colgrave, M. L.; Beck, J. L.; Sheil, M. M.; Searle, M. S. *Chem. Commun.* **2002**, 556−557.
(26) Kloster, M. B. G.; Hannis, J. C.; Muddiman, D. C.; Farrell, N. *Biochem*istry **1999**, *38*, 14731−14737.
(27) Muller, J. G.; Kayser, L. A.; Paikoff, S. J.; Duarte, V.; Tang, N.; Perez, R. J.; Rokita, S. E.; Burrows, C. J. *Coord. Chem. Rev.* **1999**, *185*−*186*, 761−774.
(28) Beck, J. L.; Gupta, R.; Urathamakul, T.; Williamson, N. L.; Sheil, M. M.; Aldrich-Wright, J. R.; Ralph, S. F. *Chem. Commun.* **2003**, 626−627.
(29) Claereboudt, J.; De Spiegeleer, B.; De Bruijn, E. A.; Gijbels, R.; Claeys, M. *J. Pharm. Biomed. Anal.* **1989**, *7*, 1599−1610.
(30) Claereboudt, J.; De Spiegeleer, B.; Lippert, B.; De Bruijn, E. A.; Claeys, M. *Spectroscopy* **1989**, *7*, 91−112.
(31) Costello, C. E.; Comess, K. M.; Plaziak, A. S.; Bancroft, D. P.; Lippard, S. J. *Int. J. Mass Spectrom. Ion Processes* **1992**, *102*, 255−279.
(32) Costello, C. E.; Nordhoff, E.; Hillenkamp, F. *Int. J. Mass Spectrom. Ion Processes* **1994**, *132*, 239−249.
(33) Gonnet, F.; Kocher, F.; Blais, J. C.; Bolbach, G.; Tabet, J. C.; Chottard, J. C. *J. Mass Spectrom.* **1996**, *31*, 802−809.
(34) Carte, N.; Legendre, F.; Leize, E.; Potier, N.; Reeder, F.; Chottard, J.-C.; Van Dorsselaer, A. *Anal. Biochem.* **2000**, *284*, 77−86.
(35) Iannitti-Tito, P.; Weimann, A.; Wickham, G.; Sheil, M. M. *Analyst* **2000**, *125*, 627−634.

considerable attention. These compounds were reported to exhibit carcinostatic activity by inhibiting cellular DNA replication and protein synthesis in vivo and, to a lesser extent, transcription in vitro.[36−43] Apart from the well-established preference for axial (*ax*) binding of adenine to the dirhodium unit,[44−50] recent findings in our laboratories have unequivocally established that equatorial (*eq*) purine interactions are also possible for these dirhodium units.[51−57] Model compounds with 9-ethylguanine and 9-ethyladenine revealed the existence of bridging and/or chelating bases that span the Rh−Rh bond. The full structural characterization, by NMR spectroscopy, of the dirhodium adducts with the DNA dinucleotides d(GpG),[58] d(pGpG),[59] and d(ApA)[60] has provided compelling evidence that d(GpG) and d(ApA) DNA fragments bind equatorially to the dirhodium unit with head-to-head arrangement of the bases. Moreover, preliminary MALDI MS studies have established that dirhodium bis-acetate units form adducts with **AA**- and **GG**-containing DNA dodecamers.[61]

Table 1. Single-Stranded Oligonucleotides Studied with Platinum and Dirhodium Compounds

oligonucleotide length	sequence
tetramers	d(C**AA**C)
	d(T**GG**T)
octamers	d(TTC**AA**CTC)
	d(TCT**GG**TCT)
dodecamers	d(CCTTC**AA**CTCTC)
	d(CCTCT**GG**TCTCC)
	d(CCTCT**AG**TCTCC)
	d(CCTCT**GA**TCTCC)

The versatility of binding modes of the nucleobases to the dirhodium core[44−60] (monodentate, bridging, and chelating) and the presence of multiple target sites on the DNA, prompted us to use MS to efficiently screen and evaluate a large number of dirhodium−DNA reactions using minimal quantities of compounds. The reactions of three dirhodium compounds, namely, $[Rh_2(O_2CCH_3)_2(CH_3CN)_6]^{2+}$ (**1**), $Rh_2(O_2CCH_3)_4$ (**2**), and $Rh_2(O_2CCF_3)_4$ (**3**) (Scheme 1), with single-stranded oligonucleotides of different lengths (tetra- to dodecamers) containing dipurine sites (**AA**, **AG**, **GA**, and **GG**) (Table 1) were monitored by MALDI and ESI MS. The relative reactivity of the dirhodium compounds was compared to the reactivity of the platinum complexes *cis*-$[Pt(NH_3)_2Cl_2]$ (cisplatin (**4**)), *cis*-$[Pt(NH_3)_2(OH_2)_2]^{2+}$ (activated cisplatin (**5**)), and $Pt(C_6H_6O_4)(NH_3)_2$ (carboplatin (**6**)) (Scheme 1). The effects of the oligonucleotide length and the nature of the dipurine sites have been evaluated for each dirhodium compound. In addition, collision-induced dissociation (CID) MS−MS was used to identify the binding site of the **GG** oligonucleotides (tetra- to dodecamers) to the metal, whereas the HPLC-purified adduct [d(CCTTC**AA**CTCTC) + $Rh_2(O_2CCH_3)_2$ − 2H] was characterized by CID MS−MS and enzymatic digestion[62−66] followed by MALDI and ESI MS. Both MALDI and ESI MS proved to be complementary, valuable tools for surveying the chemistry of dinuclear metal−DNA adducts. Although MALDI was used to rapidly screen a large number of crude dirhodium samples, the application of "soft" ionization ESI processes[67] in studying dirhodium−DNA interactions is unprecedented to our knowledge and has allowed for the identification of key metal−DNA adducts.

Materials and Methods

The compounds *cis*-$[Pt(NH_3)_2Cl_2]$ and $Pt(C_6H_6O_4)(NH_3)_2$ were obtained from Aldrich. The matrixes 3-hydroxypicolinic,[68] anthranilic, and nicotinic acids as well as the additives spermidine,

(36) Erck, A.; Rainen, L.; Whileyman, J.; Chang, I.; Kimball, A. P.; Bear, J. L. *Proc. Soc. Exp. Biol. Med.* **1974**, *145*, 1278−1282.
(37) Bear, J. L.; Gray, H. B., Jr.; Rainen, L.; Chang, I. M.; Howard, R.; Serio, G.; Kimball, A. P. *Cancer Chemother. Rep.* **1975**, *59*, 611−620.
(38) Howard, R. A.; Sherwood, E.; Erck, A.; Kimball, A. P.; Bear, J. L. *J. Med. Chem.* **1977**, *20*, 943−946.
(39) Bear, J. L.; Howard, R. A.; Dennis, A. M. *Curr. Chemother.* **1978**, 1321−1323.
(40) Howard, R. A.; Kimball, A. P.; Bear, J. L. *Cancer Res.* **1979**, *39*, 2568−2573.
(41) Rao, P. N.; Smith, M. L.; Pathak, S.; Howard, R. A.; Bear, J. L. *J. Natl. Cancer Inst.* **1980**, *64*, 905−911.
(42) Bear, J. L. In *Precious Metals 1985*, Proceedings of the Ninth International Precious Metals Conference; Zysk, E. D., Bonucci, J. A., Eds.; Int. Precious Metals: Allentown, PA, 1986; pp 337−344.
(43) (a) Sorasaenee, K.; Fu, P. K.-L.; Angeles-Boza, A. M.; Dunbar, K. R.; Turro, C. *Inorg. Chem.* **2003**, *42*, 1267−1271. (b) Chifotides, H. T.; Fu, P. K.-L.; Dunbar, K. R.; Turro, C. *Inorg. Chem.* **2004**, *43*, 1175−1183.
(44) Rainen, L.; Howard, R. A.; Kimball, A. P.; Bear, J. L. *Inorg. Chem.* **1975**, *14*, 2752−2754.
(45) Pneumatikakis, G.; Hadjiliadis, N. *J. Chem. Soc., Dalton Trans.* **1979**, 596−599.
(46) Farrell, N. *J. Chem. Soc., Chem. Commun.* **1980**, 1014−1016.
(47) Aoki, K.; Salam, M. A. *Inorg. Chim. Acta* **2002**, *339*, 427−437.
(48) Farrell, N. *J. Inorg. Biochem.* **1981**, *14*, 261−265.
(49) Rubin, J. R.; Sundaralingam, M. *J. Biomol. Struct. Dyn.* **1984**, *2*, 525−530.
(50) Rubin, J. R.; Haromy, T. P.; Sundaralingam, M. *Acta Crystallogr., Sect. C* **1991**, *47*, 1712−1714.
(51) Dunbar, K. R.; Matonic, J. H.; Saharan, V. P.; Crawford, C. A.; Christou G. *J. Am. Chem. Soc.* **1994**, *116*, 2201−2202.
(52) Day, E. F.; Crawford, C. A.; Folting, K.; Dunbar, K. R.; Christou, G. *J. Am. Chem. Soc.* **1994**, *116*, 9339−9340.
(53) Crawford, C. A.; Day, E. F.; Saharan, V. P.; Folting, K.; Huffman, J. C.; Dunbar, K. R.; Christou, G. *Chem. Commun.* **1996**, 1113−1114.
(54) Catalan, K. V.; Mindiola, D. J.; Ward, D. L.; Dunbar, K. R. *Inorg. Chem.* **1997**, *36*, 2458−2460.
(55) Catalan, K. V.; Hess, J. S.; Maloney, M. M.; Mindiola, D. J.; Ward, D. L.; Dunbar, K. R. *Inorg. Chem.* **1999**, *38*, 3904−3913.
(56) Prater, M. E.; Mindiola, D. J.; Ouyang, X.; Dunbar, K. R. *Inorg. Chem. Commun.* **1998**, *1*, 475−477.
(57) Phillips, S. L.; Christou, G.; Huffman, J. C.; Olmstead, M. M. *Abstr. Pap. Am. Chem. Soc.* **2001**, *221*, INOR-524.
(58) Chifotides, H. T.; Koshlap, K. M.; Pérez, L. M.; Dunbar, K. R. *J. Am. Chem. Soc.* **2003**, *125*, 10703−10713.
(59) Chifotides, H. T.; Koshlap, K. M.; Pérez, L. M.; Dunbar, K. R. *J. Am. Chem. Soc.* **2003**, *125*, 10714−10724.
(60) Chifotides, H. T.; Dunbar, K. R., to be submitted for publication, 2004.
(61) Asara, J. M.; Hess, J. S.; Lozada, E.; Dunbar, K. R.; Allison, J. *J. Am. Chem. Soc.* **2000**, *122*, 8−13.
(62) Zhang, L.-K.; Rempel, D.; Gross, M. L. *Anal. Chem.* **2001**, *73*, 3263−3273.
(63) Wu, H.; Aboleneen, H. *Anal. Biochem.* **2001**, *290*, 347−352.
(64) Bentzley, C. M.; Johnston, M. V.; Larsen, B. S.; Gutteridge, S. *Anal. Chem.* **1996**, *68*, 2141−2146.
(65) Smirnov, I. P.; Roskey, M. T.; Juhasz, P.; Takach, E. J.; Martin, S. A.; Haff, L. A. *Anal. Biochem.* **1996**, *238*, 19−25.
(66) Bartolini, W. P.; Bentzley, C. M.; Johnston, M. V.; Larsen, B. S. *J. Am. Soc. Mass Spectrom.* **1999**, *10*, 521−528.
(67) Cole, R. B., Ed. *Electrospray Ionization Mass Spectrometry*; Wiley: New York, 1997.
(68) Wu, K. J.; Steding, A.; Becker, C. H. *Rapid Commun. Mass Spectrom.* **1993**, *7*, 142−146.

ammonium acetate, and diammonium hydrogencitrate[69−74] were purchased from Sigma. HPLC-grade acetonitrile was obtained from Merck. MilliQ-grade water was used in all cases.

Activated cisplatin, *cis*-$[Pt(NH_3)_2(OH_2)_2]^{2+}$, was prepared by reacting an aqueous solution of cisplatin with 1.97 equiv of $AgNO_3$ for 1 day, at room temperature, in the dark. The reaction mixture was centrifuged for 10 min (Jouan A12-14 microcentrifuge) to remove AgCl. The aqueous layer was separated and centrifuged for another 10 min. This process was repeated twice, and the aqueous layer was used to react with the oligonucleotides.[75] $[Rh_2(O_2CCH_3)_2(CH_3CN)_6](BF_4)_2$ was synthesized according to literature procedures.[76]

DNA oligonucleotides were obtained from the Gene Technologies Lab at Texas A&M University (College Station, TX) or Midland Certified Reagent Company (Midland, TX). The oligonucleotides were purchased as the crude DMT (5′-*O*-dimethoxytrityl)-protected material and were purified by using Sep-Pak (Waters, Milford, MA) or Poly-Pak II (Glen Research, Sterling, VA) cartridges unless otherwise stated. After flushing the incomplete ("failure") sequences with dilute ammonium hydroxide (20%) or CH_3CN (15% in triethylammonium acetate) solutions and cleavage of the DMT group with 2% trifluoroacetic acid, the desired oligonucleotides were eluted with 20% acetonitrile and concentrated to dryness (Jouan RC 10.10 centrifugal evaporator equipped with an RCT 60 refrigerated trap). The eluted oligonucleotides were detected by UV spectroscopy (Shimadzu UV 1601PC spectrophotometer) at 260 nm. The typical oligonucleotide−metal complex ratio was 1:2, and the final concentration of the oligonucleotide was 25 pmol/μL. The metal−DNA reaction mixtures were incubated at 37 °C.

HPLC separations were performed on a Beckman Coulter System Gold instrument equipped with a 168 diode array detector. The DNA adducts were purified on a Dionex DNApac PA-100 anion-exchange column using the following mobile phase: 25 mM ammonium acetate in a CH_3CN/H_2O (10/90%) solution (eluant A) and A + 1.0 M NaCl (eluant B). The gradient employed was 20 to 35% B over 30 min and 30 to 100% B over the next 20 min. The samples were reduced in volume and desalted on a Sephadex G-25 size-exclusion column (Amersham Pharmacia Biotech, Piscataway, NJ).

Enzymatic digestion experiments were carried out using phosphodiesterase I from *Crotallus adamanteus* venom (SVP) (3′ → 5′ DNA exonuclease) and phosphodiesterase II from bovine spleen (BSP) (5′ → 3′ DNA exonuclease); both enzymes were obtained from Sigma. Phosphodiesterase I (SVP) digestions were performed using 0.2 munits of enzyme per 100 pmol of DNA oligonucleotide at room temperature with no additional buffer. Phosphodiesterase II (BSP) digestions were performed using 1.0 munit of enzyme per 100 pmol of DNA oligonucleotide at 37 °C with no additional buffer.

Table 2. Nominal Mass Differences and Numerical Designations of Dirhodium Adducts Observed by MALDI and ESI MS

composition (nominal mass difference)	numerical designation
[M] (native DNA)	I
$[M + Rh_2 - 4H]$ (202)	II
$[M + Rh_2(O_2CCH_3) - 3H]$ (262)	III
$[M + Rh_2(O_2CCH_3)_2 - 2H]$ (322)	IV
$[M + Rh_2(O_2CCH_3)(CH_3CN)_2 - 3H]$ (344)	V
$[M + Rh_2(O_2CCH_3)_2(CH_3CN)_2 - 2H]$ (404)	VI
$[M + Rh_2(O_2CCH_3)_2(CH_3CN)_4 - 2H]$ (486)	VII
$[M + Rh_2(O_2CCH_3)_3 - H]$ (382)	VIII
$[M + Rh_2(O_2CCH_3)_4]$ (442)	IX

MALDI mass spectra were acquired using an Applied Biosystems Voyager Elite XL (Framingham, MD) equipped with delayed extraction[77] and an Applied Biosystems Voyager DE STR. Negative-ion spectra were acquired in reflected mode from dried-droplet depositions of 3-hydroxypicolinic acid with diammonium hydrogencitrate additive for the platinum−DNA adducts. Negative-ion-mode spectra were acquired in linear mode using dried-droplet depositions of 80% anthranilic acid (40 mg/mL) and 20% nicotinic acid (10 mg/mL) with spermidine additive (10 mM) for the dirhodium adducts.[61,78−80] Spermine was not used because it has the same nominal mass (202 Da) as the mass difference of $\{[M + Rh_2 - 4H] - [M]\}$ ($\Delta m/z = 202$; Table 2).

Electrospray mass spectra were acquired on an MDS Sciex API QStar Pulsar (Toronto, Ontario, Canada)[81] fitted with a Protana (Odense, Denmark) nanoelectrospray source.[82] All spectra were acquired in negative-ion mode from 50% H_2O and 50% 2-propanol with 5 mM ammonium acetate. The spray voltage was between −1050 and −1100 V. The nozzle−skimmer potential was set to −5 V to minimize fragmentation in that region. MS−MS was performed by collision-induced dissociation (CID) using N_2 target gas over a range of different voltages ($E_{lab} = 80-240$ eV).

In the graphs of reaction progress (e.g., Figures 4 and 5), the product-ion abundance is the sum of all of the product-ion peak areas (all ion signals containing the metal center) compared to the sum of all ions containing DNA, including unreacted DNA (summation of all of the dirhodium species/total signal × 100). The error bars in Figures S1B, S7, and S8 of the Supporting Information were determined from three to six independent measurements of the product-ion signal peak areas for each reaction and time point. The average was plotted, and the error bars represent the standard deviation of the total product-ion signal peak area.

Results

I. Characterization of Various Metalated Adducts. a. Metal−DNA Adducts Observed by MALDI MS. The

(69) Zhu, Y. F.; Taranenko, N. I.; Allman, S. L.; Martin, S. A.; Haff, L.; Chen, C. H. *Rapid Commun. Mass Spectrom.* **1996**, *10*, 1591−1596.
(70) Li, Y. C. L.; Cheng, S.-W.; Chan, T.-W. D. *Rapid Commun. Mass Spectrom.* **1998**, *12*, 993−998.
(71) Cheng, S.-w.; Chan, T.-W. D. *Rapid Commun. Mass Spectrom.* **1996**, *10*, 907−910.
(72) Langley, G. J.; Herniman, J. M.; Davies, N. L.; Brown, T. *Rapid Commun. Mass Spectrom.* **1999**, *13*, 1717−1723.
(73) Simmons, T. A.; Limbach, P. A. *J. Am. Soc. Mass Spectrom.* **1998**, *9*, 668−675.
(74) Ragas, J. A.; Simmons, T. A.; Limbach, P. A. *Analyst* **2000**, *125*, 575−581.
(75) Takahara, P. M.; Frederick, C. A.; Lippard, S. *J. Am. Chem. Soc.* **1996**, *118*, 12309−12321.
(76) Pimblett, G.; Garner, C. D.; Clegg, W. *J. Chem. Soc., Dalton Trans.* **1986**, 1257−1263.
(77) Vestal, M. L.; Juhasz, P.; Martin, S. A. *Rapid Commun. Mass Spectrom.* **1995**, *9*, 1044−1050.
(78) Asara, J. M.; Allison, J. *Anal. Chem.* **1999**, *71*, 2866−2870.
(79) Zhu, Y. F.; Taranenko, N. I.; Allman, S. L.; Taranenko, N. V.; Martin, S. A.; Haff, L. A.; Chen. C. H. *Rapid Commun. Mass Spectrom.* **1997**, *11*, 897−903.
(80) Nordhoff, E.; Ingendoh, A.; Cramer, R.; Overberg, A.; Stahl, B.; Karas, M.; Hillenkamp, F.; Crain, P. F. *Rapid Commun. Mass Spectrom.* **1992**, *6*, 771−776.
(81) Hopfgartner, G.; Chernushevich, I. V.; Covey, T.; Plomley, J. B.; Bonner, R. *J. Am. Soc. Mass Spectrom.* **1999**, *10*, 1305−1314.
(82) Wilm, M.; Mann, M. *Anal. Chem.* **1996**, *68*, 1−8.

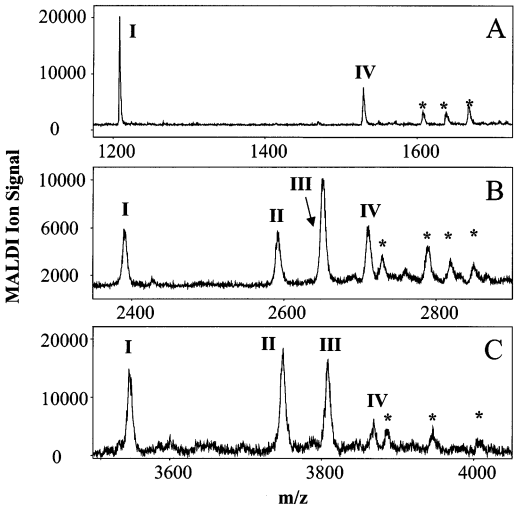

Figure 1. MALDI mass spectra of reaction mixtures for (A) d(T**GG**T), (B) d(TCT**GG**TCT), and (C) d(CCTCT**GG**TCTCC) with $[Rh_2(O_2CCH_3)_2(CH_3CN)_6]^{2+}$. The ion signals corresponding to the $[M - H]^-$ for the DNA oligonucleotide (I), $[M + Rh_2 - 5H]^-$ (II), $[M + Rh_2(O_2CCH_3) - 4H]^-$ (III), and $[M + Rh_2(O_2CCH_3)_2 - 3H]^-$ (IV) are indicated. The asterisks (*) indicate matrix adducts.

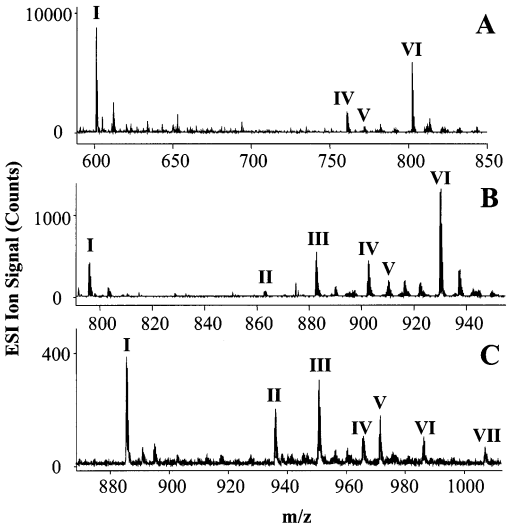

Figure 2. ESI mass spectra obtained from reaction mixtures of (A) d(T**GG**T), (B) d(TCT**GG**TCT), and (C) d(CCTCT**GG**TCTCC) with $[Rh_2(O_2CCH_3)_2(CH_3CN)_6]^{2+}$ after incubation for 9 days. The ion signals corresponding to the DNA oligonucleotide (I) and different dirhodium adducts $[M + Rh_2 - 4H]$ (II), $[M + Rh_2(O_2CCH_3) - 3H]$ (III), $[M + Rh_2(O_2CCH_3)_2 - 2H]$ (IV), $[M + Rh_2(O_2CCH_3)(CH_3CN)_2 - 3H]$ (V), $[M + Rh_2(O_2CCH_3)_2(CH_3CN)_2 - 2H]$ (VI), and $[M + Rh_2(O_2CCH_3)_2(CH_3CN)_4 - 2H]$ (VII) are indicated. The species in spectra A, B, and C have ionization charged states of −2, −3, and −4, respectively.

negative-ion MALDI mass spectra of activated cisplatin, cisplatin, and carboplatin are dominated by a single ion that corresponds to $[M + Pt(NH_3)_2 - 3H]^-$ (Supporting Information, Figure S1). Conversely, the MS spectra of the dirhodium reaction products reveal that the chemistry is significantly more complicated. The dirhodium adducts encountered in the present study, along with their nominal mass differences and numerical designations, are listed in Table 2. The MALDI MS spectrum of the reaction products of $[Rh_2(O_2CCH_3)_2(CH_3CN)_6]^{2+}$ with d(T**GG**T) exhibits only the bis-acetate $[d(T\mathbf{GG}T) + Rh_2(O_2CCH_3)_2 - 3H]^-$ (IV) ion (Figure 1A), whereas for the corresponding octa- and dodecamers, the monoacetate $[M + Rh_2(O_2CCH_3) - 4H]^-$ (III) and the Rh_2(II, II) core adducts $[M + Rh_2 - 5H]^-$ (II) are present (Figure 1B and C). Similar trends are observed for the reactions of $Rh_2(O_2CCH_3)_4$ with **GG** oligonucleotides of increasing length.

In the MALDI MS of the $Rh_2(O_2CCF_3)_4$ reactions with d(T**GG**T), d(TCT**GG**TCT), and d(CCTCT**GG**TCTCC), the dominant ion signal corresponds to $[M + Rh_2 - 5H]^-$ (II) (Supporting Information, Figure S2). Similar trends are observed for the reactions of the previous dirhodium complexes with **AA**-containing oligonucleotides, that is, d(C**AA**C), d(TTC**AA**CTC), and d(CCTTC**AA**CTCTC).

b. Metal−DNA Adducts Observed by ESI MS. The ESI MS spectra of the platinum reactions exhibit the platinated DNA oligonucleotide ions corresponding to $[M + Pt(NH_3)_2 - 3H]^-$, and the initial outer-sphere adducts between the DNA oligonucleotides and cisplatin ($[M + Pt(NH_3)_2Cl_2]$) or carboplatin ($[M + Pt(C_6H_6O_4)(NH_3)_2]$) are observed as well.[34]

The ESI mass spectra acquired from reaction mixtures of $[Rh_2(O_2CCH_3)_2(CH_3CN)_6]^{2+}$ incubated with **GG**- and **AA**-containing oligonucleotides are shown in Figures 2 and S3 (Supporting Information). The dominant adduct observed in the reactions with d(T**GG**T) and d(TCT**GG**TCT) corresponds to $[M + Rh_2(O_2CCH_3)_2(CH_3CN)_2 - 2H]$ (VI) (Figure 2A and B), whereas reactions with d(CCTCT**GG**TCTCC) mostly yield $[M + Rh_2(O_2CCH_3) - 4H]^-$ (III) (Figure 2C) after 9 days of incubation. Conversely, reactions of d(C**AA**C), d(TTC**AA**CTC), and d(CCTTC**AA**CTCTC) (Supporting Information, Figure S3B) yield comparable quantities of all possible dirhodium adducts. The ion signals for the electrostatic outer-sphere adducts $[M + Rh_2(O_2CCH_3)_2(CH_3CN)_6]$ and $[M + Rh_2(O_2CCH_3)_2(CH_3CN)_4(H_2O)_2]$ were not observed.

The ESI mass spectra of the reaction of $Rh_2(O_2CCH_3)_4$ incubated with **GG** and **AA** oligonucleotides exhibit the $[M + Rh_2(O_2CCH_3)_2 - 2H]$, $[M + Rh_2(O_2CCH_3)_3 - H]$, and $[M + Rh_2(O_2CCH_3)_4]$ adducts for the tetramers, whereas the spectra for the octamers show the monoacetate ion $[M + Rh_2(O_2CCH_3) - 4H]^-$. The dominant species for the $Rh_2(O_2CCH_3)_4$ reaction with the octamers d(TTC**AA**CTC) and d(TCT**GG**TCT) are $[M + Rh_2(O_2CCH_3)_3 - H]$ (VIII) (Supporting Information, Figure S4A) and $[M + Rh_2(O_2CCH_3)_2 - 2H]$ (IV) (Supporting Information, Figure S4B), respectively, whereas for the d(CCTTC**AA**CTCTC) and d(CCTCT**GG**TCTCC) dodecamers, the $[M + Rh_2(O_2CCH_3)_2 - 2H]$ (IV) (Supporting Information, Figure S5A) and $[M + Rh_2(O_2CCH_3) - 3H]$ (III) (Supporting Information, Figure S5B) adducts dominate, respectively.

The ESI mass spectra of $Rh_2(O_2CCF_3)_4$ with d(CCTCT**GG**TCTCC) reveal the preferential formation of $[M + Rh_2 - 4H]$ (II) (Supporting Information, Figure S6C).

c. MALDI and ESI Spectra of the HPLC-Purified Dirhodium Adduct $[Rh_2(O_2CCH_3)_2$ + d(CCTTCAACTCTC)]. From the reaction between $Rh_2(O_2CCH_3)_4$ and d(CCTTC**AA**CTCTC), the dirhodium bis-acetate species $[M + Rh_2(O_2CCH_3)_2 - 2H]$ (IV) was isolated by anion-exchange HPLC. In the MALDI mass spectrum of the adduct at the

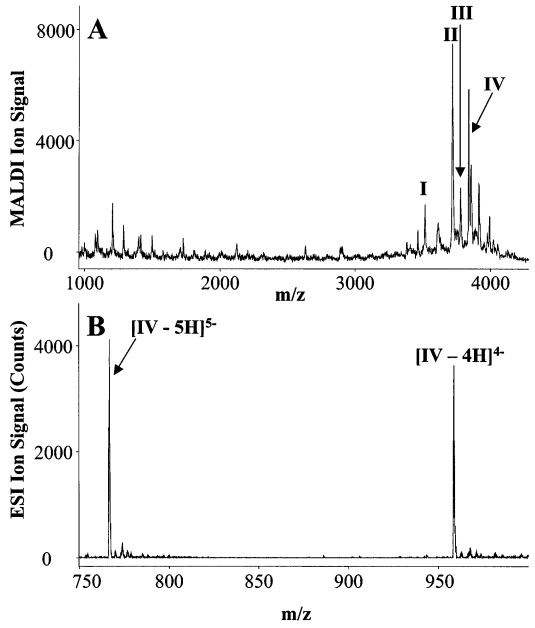

Figure 3. (A) MALDI and (B) ESI mass spectra of the HPLC-purified dirhodium bis-acetate DNA adduct [M + $Rh_2(O_2CCH_3)_2$ − 2H]. The ion signals corresponding to the DNA oligonucleotide (I) and various dirhodium adducts [M + Rh_2 − 4H] (II), [M + $Rh_2(O_2CCH_3)$ − 3H] (III), and [M + $Rh_2(O_2CCH_3)_2$ − 2H] (IV) are indicated. The ions correspond to −4 charged species.

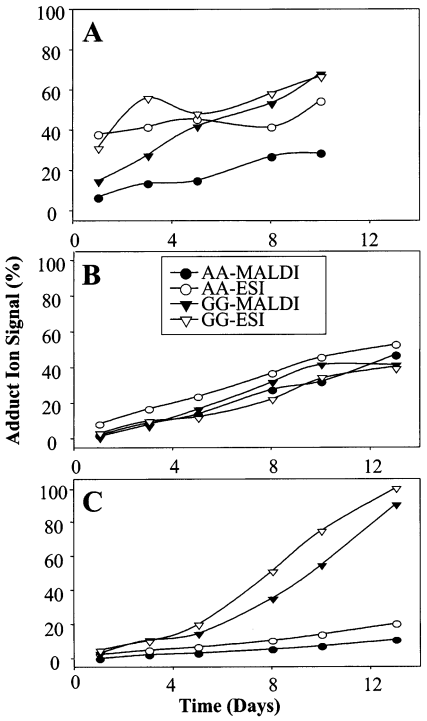

Figure 4. Reaction progress monitored by MALDI (closed symbols) and ESI (open symbols) for reactions of (A) $[Rh_2(O_2CCH_3)_2(CH_3CN)_6]^{2+}$, (B) $Rh_2(O_2CCH_3)_4$, and (C) $Pt(C_6H_6O_4)(NH_3)_2$ with the oligonucleotides d(CCTTC**AA**CTCTC) (circles) and d(CCTCT**GG**TCTCC) (triangles).

threshold laser fluence, numerous ion signals are present (Figure 3A; ions I−IV), and at high laser power, further fragmentation occurs. In the ESI MS spectra, the dominant ion signals correspond to different charged states of the [M + $Rh_2(O_2CCH_3)_2$ − 2H] (IV) adduct (Figure 3B).

II. Kinetics of the Metal−DNA Reactions Monitored by MS. a. Metal−DNA Reactions Monitored by MALDI MS. The intensities of the ion signals corresponding to the dirhodium adducts [M + Rh_2 − 5H]$^-$ (II), [M + $Rh_2(O_2CCH_3)$ − 4H]$^-$ (III), and [M + $Rh_2(O_2CCH_3)_2$ − 3H]$^-$ (IV) are summed, and the adduct formation is expressed as a percentage of the total ion intensity (Figures 4 and S7 (Supporting Information)).

The analysis of the adduct ion signals observed by MALDI MS indicates that the metal complexes under study can be separated in two groups on the basis of their relative rates of reaction; $[Pt(NH_3)_2(OH_2)_2]^{2+}$, $Rh_2(O_2CCF_3)_4$, and *cis*-$[Pt(NH_3)_2Cl_2]$ require several hours, whereas $[Rh_2(O_2CCH_3)_2(CH_3CN)_6]^{2+}$, $Rh_2(O_2CCH_3)_4$, and $Pt(C_6H_6O_4)(NH_3)_2$ require several days for the reaction with the dodecamers to be completed (Supporting Information, Figure S8). The observed trend is that dodecamers and octamers react faster than tetramers for a given metal complex and the same dipurine binding site (except for the case of $[Rh_2(O_2CCH_3)_2(CH_3CN)_6]^{2+}$, which reacts faster with the **GG** octamers than with the dodecamers; Figures 1 and 2).

MS studies of reaction mixtures for $[Rh_2(O_2CCH_3)_2(CH_3CN)_6]^{2+}$, $Rh_2(O_2CCH_3)_4$, and $Pt(C_6H_6O_4)(NH_3)_2$ with the **AA**, **AG**, **GA**, and **GG** dodecamers were performed, and a plot of the MALDI ion signal versus time for the **AA** and **GG** oligonucleotides is shown in Figure 4. For $[Rh_2(O_2CCH_3)_2(CH_3CN)_6]^{2+}$, the **GG** dodecamer reacts the fastest, whereas no appreciable difference in reactivity is observed for the **AA**-, **AG**-, and **GA**-containing sequences (Supporting Information, Figure S7A). As determined by MALDI, the reactivity of the **GG** oligonucleotide with $Rh_2(O_2CCH_3)_4$ (Supporting Information, Figure S7B) is enhanced by ∼2% compared to that of the **AA** oligomer; furthermore, the homopurine sequences have comparable reaction rates with the **AG** and **GA** sequences for $Rh_2(O_2CCH_3)_4$. In the carboplatin reactions, all of the previous oligonucleotides react at a similar rate, except for the **AA**-containing strand (Supporting Information, Figure S7C).

The reactions of $Rh_2(O_2CCF_3)_4$ with the **AA**, **GG**, **AG**, or **GA** dodecamers proceed with an enhanced reactivity of the **GG** compared to the **AA** dodecamer, whereas the **AG** and **GA** sequences have comparable rates among them but react slower than the **AA** and **GG** strands (Supporting Information, Figure S9).

b. Metal−DNA Reactions Monitored by ESI MS. ESI MS was used to study the relative reaction rates of $[Rh_2(O_2CCH_3)_2(CH_3CN)_6]^{2+}$, $Rh_2(O_2CCH_3)_4$, and $Pt(C_6H_6O_4)(NH_3)_2$ with **AA**, **GG**, **AG**, and **GA** dodecamers. Plots of the ion signal for the metalated adducts versus time are shown in Figures 4 and S10 (Supporting Information). For the $[Rh_2(O_2CCH_3)_2(CH_3CN)_6]^{2+}$ reactions, the **GG** dodecamer is the most reactive, followed by the **AA** strand and oligonucleotides containing heteropurine sites (Figures 4A and S10A (Supporting Information)). Conversely, the ESI adduct ion signal of the reactions with $Rh_2(O_2CCH_3)_4$ is higher for the **AA** dodecamer (Figure 4B and S10B (Supporting Information)). When the $Rh_2(O_2CCH_3)_4$ reactions are monitored by ESI MS for the **AA** and **GG** dodecamers, the most abundant adducts are [M + $Rh_2(O_2CCH_3)_2$ − 2H] (IV) (Figures 5A

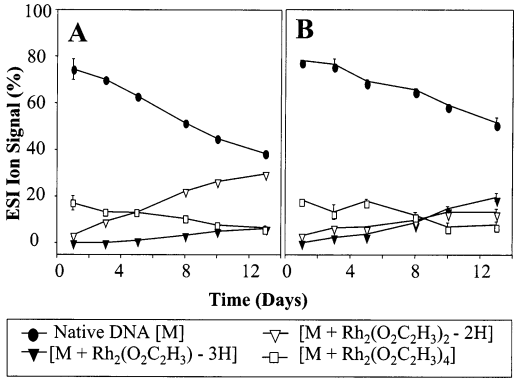

Figure 5. ESI MS monitoring of individual adduct formation in reactions of $Rh_2(O_2CCH_3)_4$ with (A) d(CCTTC**AA**CTCTC) and (B) d(CCTCT**GG**TCTCC).

and S5A (Supporting Information)) and [M + $Rh_2(O_2CCH_3)$ − 3H] (III) (Figures 5B and S5B (Supporting Information)), respectively.

III. Metal−DNA Adduct Stability and Metal Binding Site Identification by MS. a. Adduct Stability and Binding Mechanism Probed by ESI CID MS−MS Fragmentation. The relative stability of the various dirhodium−DNA adducts and the relative binding strength of the ligands, that is, acetate, acetonitrile, and DNA oligonucleotides, were probed by CID MS−MS.

ESI CID MS−MS studies were performed on the [M + $Rh_2(O_2CCH_3)_2(CH_3CN)_4$ − 2H], [M + $Rh_2(O_2CCH_3)_2(CH_3CN)_2$ − 2H], [M + $Rh_2(O_2CCH_3)_2$ − 2H], [M + $Rh_2(O_2CCH_3)$ − 3H], and [M + Rh_2 − 4H] adducts obtained from the reaction of $[Rh_2(O_2CCH_3)_2(CH_3CN)_6]^{2+}$ with DNA. CID MS−MS spectra of ion signals corresponding to [d(T**GG**T) + $Rh_2(O_2CCH_3)_2(CH_3CN)_4$ − 4H]$^{2-}$, [d(TCT**GG**TCT) + $Rh_2(O_2CCH_3)_2(CH_3CN)_4$ − 4H]$^{2-}$, and [d(CCTCT**GG**TCTCC) + $Rh_2(O_2CCH_3)_2(CH_3CN)_4$ − 4H]$^{2-}$ are shown in Figure 6A−C, respectively. In all cases, the loss of acetonitrile groups is considerably greater than the loss of acetate ligands.

CID MS−MS spectra of [d(TTC**AA**CTC) + $Rh_2(O_2CCH_3)_4$ − 3H]$^{3-}$ and [d(TTC**AA**CTC) + $Rh_2(O_2CCH_3)_3$ − 4H]$^{3-}$ ions produced from the reaction between $Rh_2(O_2CCH_3)_4$ and d(TTC**AA**CTC) are shown in Figure 6D and E, respectively. Under the conditions used for MS, a minimal loss of acetate groups was observed (<3% of the total ion signal), whereas in the CID MS−MS of [M + $Rh_2(O_2CCH_3)_3$ − 4H]$^{3-}$ adducts at slightly higher energy, ion signals [M + $Rh_2(O_2CCH_3)_2$ − 4H]$^{2-}$ (IV) corresponding to the loss of one acetate are the only ones observed. Similar observations were made for all the oligonucleotides studied regardless of length or central dipurine site.

b. Metal Binding Site Identification. i. MALDI In-Source Decay Fragmentation (ISD). In-source decay fragmentation (ISD) induces fragmentation along the DNA phosphodiester backbone and produces ions with free 5′ hydroxyl (y ions) or 5′ phosphate groups (w ions).[83] Although metal−DNA adduct ions preferentially fragment by cleavage

(83) Nordhoff, E.; Kirpekar, F.; Roepstorff, P. *Mass Spectrom. Rev.* **1996**, *15*, 67−138.

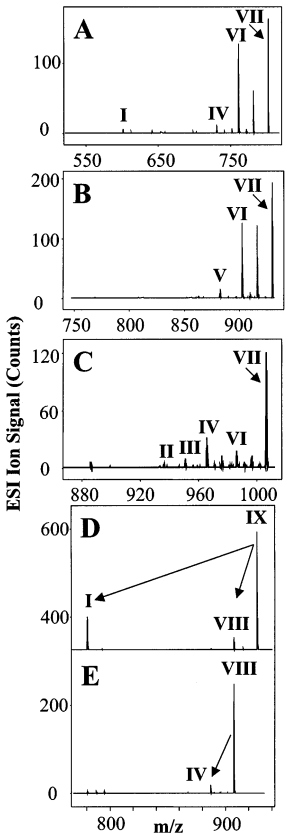

Figure 6. Product ion spectra obtained from CID MS−MS of (A) [d(T**GG**T) + $Rh_2(O_2CCH_3)_2(CH_3CN)_4$ − 4H]$^{2-}$, (B) [d(TCT**GG**TCT) + $Rh_2(O_2CCH_3)_2(CH_3CN)_4$ − 5H]$^{3-}$, and (C) [d(CCTCT**GG**TCTCC) + $Rh_2(O_2CCH_3)_2(CH_3CN)_4$ − 6H]$^{4-}$ under the same conditions used for MS. Product ion spectra obtained from CID MS−MS of [d(TTC**AA**CTC) + $Rh_2(O_2CCH_3)_4$ − 3H]$^{3-}$ (D) and [d(TTC**AA**CTC) + $Rh_2(O_2CCH_3)_3$ − 4H]$^{3-}$ (E). The ion signals corresponding to the DNA oligonucleotide (I) and different dirhodium adducts, [M + Rh_2 − 4H] (II), [M + $Rh_2(O_2CCH_3)$ − 3H] (III), [M + $Rh_2(O_2CCH_3)_2$ − 2H] (IV), [M + $Rh_2(O_2CCH_3)(CH_3CN)_2$ − 3H] (V), [M + $Rh_2(O_2CCH_3)_2(CH_3CN)_2$ − 2H] (VI), [M + $Rh_2(O_2CCH_3)_2(CH_3CN)_4$ − 2H] (VII), [M + $Rh_2(O_2CCH_3)_3$ − H] (VIII), and [M + $Rh_2(O_2CCH_3)_4$] (IX), are depicted.

of the phosphodiester backbone adjacent to the dipurine site, it is not possible to use ISD techniques for direct identification of the metal binding sites to DNA because the resulting ISD fragment ions lose the metal center prior to phosphate backbone cleavage (Supporting Information, Figure S11).

ii. CID MS−MS Fragmentation. CID MS−MS was applied to the dirhodium adducts with **AA** and **GG** dodecamers.

AA Dodecamer. The fragment ions of [d(CCTTC**AA**CTCTC) + $Rh_2(O_2CCH_3)_2$ − 7H]$^{5-}$ (IV) correspond to d(CCTTCAp) or d(pACTCTC) (when fragmentation occurs from the 5′ and 3′ ends, respectively) as well as d(CCTTC**AA**p) or d(p**AA**CTCTC) segments of the native strand (the fragment $C_3T_2A_2$ exhibits higher intensity than the C_3T_2A fragment, Figure 7A); that is, fragmentation occurs adjacent to or between the A bases, but the fragments are not metalated.

GG Dodecamer. CID MS−MS fragmentation of [d(CCTCT**GG**TCTCC) + $Rh_2(O_2CCH_3)_2$ − 2H] produces an ion signal corresponding to [M + $Rh_2(O_2CCH_3)_2$ − C_3T_2 − 5H]$^{3-}$ (Figure 7B). The observed fragment ions d(CCTCTp)

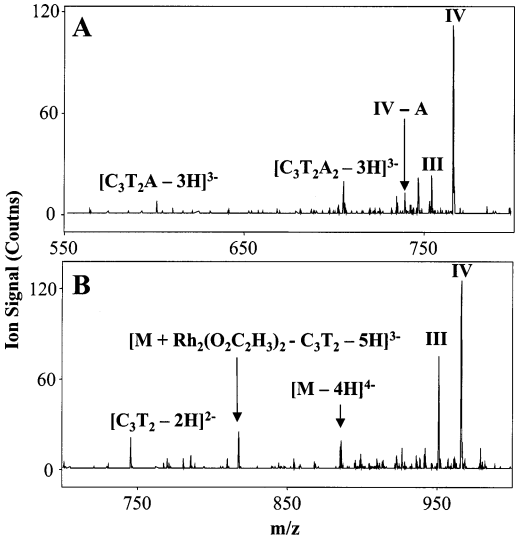

Figure 7. Product ion spectra obtained from CID MS−MS of (A) [d(CCTTC**AA**CTCTC) + $Rh_2(O_2CCH_3)_2$ − 7H]$^{5-}$ and (B) [d(CCTCT**GG**TCTCC) + $Rh_2(O_2CCH_3)_2$ − 6H]$^{4-}$. The ion signals corresponding to different charged states of [M + $Rh_2(O_2CCH_3)$ − 3H] (III) and [M + $Rh_2(O_2CCH_3)_2$ − 2H] (IV) are indicated. The nonmetalated DNA fragments contain terminal phosphate groups. Fragmentation may occur from the 5′ and 3′ ends of the oligonucleotide.

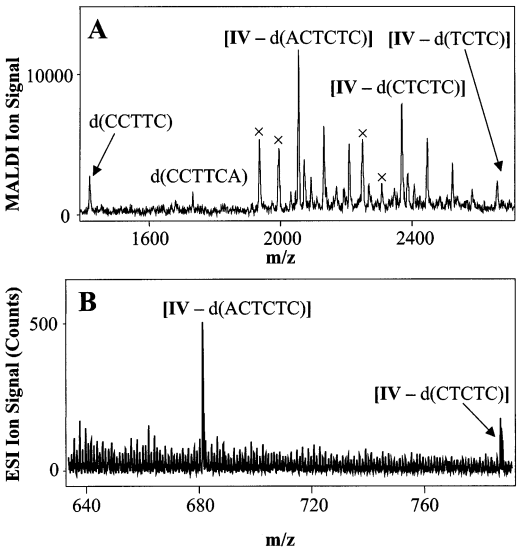

Figure 8. (A) MALDI MS and (B) ESI MS spectra of the enzymatic digestion products of [d(CCTTC**AA**CTCTC) + $Rh_2(O_2CCH_3)_2$ − 2H] (IV) by phosphodiesterase I for 2.5 h. The ion signal observed in ESI MS is low because of the buffer used for the enzymatic digestion. Fragment ions corresponding to the loss of acetate are labeled with (×).

or d(pTCTCC) of the native strand are produced by fragmentation adjacent to the **GG** dipurine site.

iii. Enzymatic Digestions Followed by MALDI and ESI MS. Exonuclease digestions followed by MS analysis of an HPLC fraction that corresponds to the bisacetate adduct [d(CCTTC**AA**CTCTC) + $Rh_2(O_2CCH_3)_2$] (identified by MS), was used to probe the dodecamer binding site to the dirhodium unit. After digestion of the [d(CCTTC**AA**CTCTC) + $Rh_2(O_2CCH_3)_2$ − 2H] (IV) adduct by phosphodiesterase I, in the MALDI (Figure 8A) and ESI MS (Figure 8B) spectra, the ion signals correspond to the cleavage of d(CTCTC) and d(ACTCTC) fragments from the 3′ end of the [$Rh_2(O_2CCH_3)_2$ + d(CCTTC**AA**CTCTC) − 2H] (IV) adduct. In the MALDI spectrum, the cleavage of the d(TCTC) fragment is also observed. After digestion of the [d(CCTTC**AA**CTCTC) + $Rh_2(O_2CCH_3)_2$ − 2H] adduct by phosphodiesterase II, in the MALDI (Figure S12A) and ESI MS (Figure S12B) spectra, the ion signals correspond to the cleavage of d(CCTTC) and d(CCTTCA) fragments from the 5′ end of the [$Rh_2(O_2CCH_3)_2$ + d(CCTTC**AA**CTCTC) − 2H] adduct.

Discussion

Relative Reactivity of Metal Complexes Associated with Leaving Groups. The order of reactivity found from the MALDI experiments, namely, *cis*-[$Pt(NH_3)_2(OH_2)_2$]$^{2+}$ ≈ $Rh_2(O_2CCF_3)_4$ > *cis*-[$Pt(NH_3)_2Cl_2$] ≫ [$Rh_2(O_2CCH_3)_2(CH_3CN)_6$]$^{2+}$ > $Rh_2(O_2CCH_3)_4$ ≈ $Pt(C_6H_6O_4)(NH_3)_2$ (Supporting Information, Figure S8), is in accord with the relative lability of the leaving group(s) for each complex. It is well established that the rate of hydrolysis of the first chloride ion to yield the monoaquated species *cis*-[$Pt(NH_3)_2(OH_2)Cl$]$^{1+}$ is the rate-determining step for the initial binding of cisplatin to DNA; that is, the relative reactivity of *cis*-[$Pt(NH_3)_2Cl_2$] and *cis*-[$Pt(NH_3)_2(OH_2)_2$]$^{2+}$ toward DNA is correlated to the rate of hydrolysis of chloride and water (water is a better leaving group than chloride).[84−86] Carboplatin is less reactive than cisplatin (and therefore less toxic) because of the slower rate of hydrolysis of the chelating 1,1-dicarboxylato-cyclobutane dianion compared to that of the chloride ion.[85,87]

By comparison of the relative reactivities of the dirhodium adducts with those of platinum, one can ascertain the relative ease of substitution of the ligands attached to dirhodium by DNA. The comparable reaction time scale of *cis*-[$Pt(NH_3)_2(OH_2)_2$]$^{2+}$ and $Rh_2(O_2CCF_3)_4$ with DNA oligonucleotides indicates that trifluoroacetate groups are highly labile; in fact, the $Rh_2(O_2CCF_3)_4$ reaction is complete within the first day of incubation (Supporting Information, Figure S9). The enhanced lability of $CF_3CO_2^-$ compared to that of the $CH_3CO_2^-$ ligands is supported by the fact that a different number of bridging groups are retained by the dirhodium core in the reactions of $Rh_2(O_2CCF_3)_4$ (prevalent ion [M + Rh_2 − 5H]$^-$ (II)) and $Rh_2(O_2CCH_3)_4$ (prevalent ion [M + $Rh_2(O_2CCH_3)$ − 3H] (III)) with **GG** sequences (Figures S2, S5B, and S6 (Supporting Information)) and by the presence of an intense monotrifluoroacetate adduct ion peak for [M + $Rh_2(O_2CCF_3)$ − 3H]$^-$ (IIIa) observed mainly by ESI (Supporting Information, Figure S6) because of the softness of the ionization process.[67] The higher reactivity of $Rh_2(O_2CCF_3)_4$ compared to that of $Rh_2(O_2CCH_3)_4$ correlates with the increased basicity of $CH_3CO_2^-$ (pK_b 9.25) compared to that of $CF_3CO_2^-$ (pK_b > 13), which makes the latter a better

(84) Bancroft, D. P.; Lepre, C. A.; Lippard, S. J. *J. Am. Chem. Soc.* **1990**, *112*, 6860−6871.
(85) Bloemink, M. J.; Reedijk, J. In *Metal Ions in Biological Systems*; Sigel, A., Sigel, H., Eds.; Marcel Dekker: New York, 1996; Vol. 32, pp 641−685.
(86) Berners-Price, S. J.; Barnham, K. J.; Frey, U.; Sadler, P. J. *Chem.—Eur. J.* **1996**, *2*, 1283−1291.
(87) Cohen, S. M.; Lippard, S. J. *Prog. Nucl. Acid Res. Mol. Biol.* **2001**, *67*, 93−130.

leaving group,[55,88] whereas the enhanced reactivity of $[Rh_2(O_2CCH_3)_2(CH_3CN)_6]^{2+}$ compared to that of $Rh_2(O_2CCH_3)_4$, upon reaction with DNA oligonucleotides, is justified on the basis of the presence of more labile monodentate *eq* acetonitrile groups compared to bidentate acetate bridges. The latter point is further confirmed by the fact that the acetate ligands remain attached to the dirhodium core, in favor of the *eq* acetonitrile groups, during the desorption and ionization process in the MALDI mass spectra of $[Rh_2(O_2CCH_3)_2(CH_3CN)_6]^{2+}$ adducts with **GG** sequences (Figure 1); that is, no dirhodium acetonitrile-containing species are observed in the MALDI spectra. On the contrary, acetonitrile groups bound to the dirhodium core are observed in the ESI spectra (adducts V, VI, and VII; Figures 2 and S3 (Supporting Information)) owing to the soft nature of the ESI process.[67]

Effects of Oligonucleotide Length on Reactivity and Specificity of Products. The observed trend of dodecamers and octamers reacting faster than tetramers, for a given metal complex and the same purine motif (except for the case of $[Rh_2(O_2CCH_3)_2(CH_3CN)_6]^{2+}$ which reacts faster with the **GG** octamers than with the dodecamers, Figures 1 and 2) was established by MALDI MS. An enhanced rate of reactivity with increasing oligonucleotide length has been noted for platinum compounds and is attributed to initial weak preassociation (due to electrostatic interactions) between the positively charged metal species and the negatively charged phosphate backbone prior to covalent binding.[89,90]

In the cases of $Rh_2(O_2CCH_3)_4$ and $[Rh_2(O_2CCH_3)_2(CH_3CN)_6]^{2+}$, the higher observed lability of the acetate bridges with increasing oligonucleotide length (Figures 1 and 2) is attributed to steric hindrance from the acetate ligands as the accessibility of the binding sites on the DNA diminishes and greater repulsive interactions between the negatively charged acetate ligands and the DNA backbone phosphates. For $Rh_2(O_2CCF_3)_4$, the $CF_3CO_2^-$ groups are easily dissociated due to their enhanced lability, regardless of the size of the oligonucleotide (Supporting Information, Figure S2).

The observation of the $[M + Rh_2 - 4H]$ (II) adduct in the MALDI spectra of the reaction mixtures of the dodecamers (Figures 1C and 2C) indicates that the dirhodium core remains intact in the absence of carboxylates.[91]

Reaction Pathway Implied by Specific Metal Adduct Formation. In the ESI mass spectra, the presence of the $[M + Rh_2(O_2CCH_3)_4]$ (IX) ion from the oligonucleotide reactions with $Rh_2(O_2CCH_3)_4$ (Supporting Information, Figures S4 and S5) and the $[M + Rh_2(O_2CCH_3)_2(CH_3CN)_4 - 2H]$ (VII) ion from the reactions with $[Rh_2(O_2CCH_3)_2(CH_3CN)_6]^{2+}$ (Figure 2C) implies that DNA initially binds to *ax* positions of the dirhodium complexes. The appearance of ion signals corresponding to the native DNA oligonucleotide (I) in the product-ion spectra of $[M + Rh_2(O_2CCH_3)_2(CH_3CN)_4 - 5H]^{3-}$ (Figure 6A) and $[M + Rh_2(O_2CCH_3)_4 - 3H]^{3-}$ (Figure 6D), under transmission conditions, further supports initial weak DNA binding to *ax* positions of the dirhodium core. The decrease in intensity of the ion signals corresponding to the native strand (I) in the product-ion spectra of $[M + Rh_2(O_2CCH_3)_3 - 4H]^{3-}$ (Figure 6E) compared to that in the spectra of $[M + Rh_2(O_2CCH_3)_4 - 3H]^{3-}$ (Figure 6D) is consistent with initial *ax* binding of one DNA base to the dirhodium core (Scheme 2a) followed by a second DNA base attack at an *eq* site (Scheme 2b) and the possible shift of both coordinated bases to *eq* sites (Scheme 2c) with concomitant displacement of bridging carboxylate groups from *eq* positions; the latter sequence of events is further supported by product-ion signals corresponding to loss of one acetate group only in the CID MS−MS spectra of the $[M + Rh_2(O_2CCH_3)_3 - 4H]^{3-}$ ion (Figure 6E). It has precedent in the 2,2′-bipyridine (bpy)-dirhodium chemistry wherein the acetate groups are removed from the dirhodium core in multiple steps as the incoming nucleophile (bpy) eventually acquires an *eq*−*eq* binding mode.[92] It is thus logical to conclude that, for dirhodium, *ax*−*eq* or *eq*−*eq* DNA adducts are possible.

Scheme 2. Possible Sequence of Events Involved in the Reactions of Dirhodium Tetracarboxylate Compounds with DNA (a) *ax*; (b) *ax*−*eq*; (c) *eq*−*eq* Dirhodium−DNA Adducts

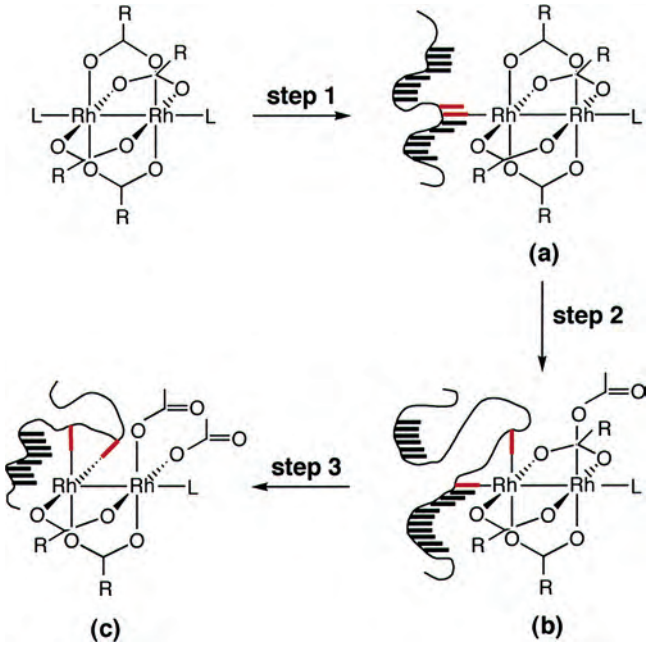

Effect of Oligonucleotide Dipurine Motif on Reactivity and Specificity of Products. For the three dirhodium compounds, especially $Rh_2(O_2CCF_3)_4$ and $[Rh_2(O_2CCH_3)_2(CH_3CN)_6]^{2+}$, the most reactive dodecamer is the one that contains a **GG** dipurine site (Supporting Information, Figures S7 and S9) (vide infra). Similar behavior was observed for cisplatin, which is likely related to the greatest Lewis basicity of the N7 position of guanine compared to the other sites on DNA.[89,93,94]

(88) Reynolds, J. D.; Burn, J. L. E.; Boggess, B.; Cook, K. D.; Woods, C. *Inorg. Chem.* **1993**, *32*, 5517−5521.
(89) Elmroth, S. K. C.; Lippard, S. J. *J. Am. Chem. Soc.* **1994**, *116*, 3633−3634.
(90) Wang, Y.; Farrell, N.; Burgess, J. D. *J. Am. Chem. Soc.* **2001**, *123*, 5576−5577.
(91) Erck, A.; Sherwood, E.; Bear, J. L.; Kimball, A. P. *Cancer Res.* **1976**, *36*, 2204−2209.
(92) Crawford, C. C.; Matonic, J. H.; Streib, W. E.; Huffman, J. C.; Dunbar, K. R.; Christou, G. *Inorg. Chem.* **1993**, *32*, 3125−3133.

The reactions between $Rh_2(O_2CCH_3)_4$ and the oligonucleotides were monitored by ESI, and it was found that the **AA** sequence is the most reactive (Figures 4 and S10 (Supporting Information)). This finding is not unexpected in light of the gentle nature of the ESI ionization process, which allows for weakly bound *ax* dirhodium−DNA **AA** dodecamers to be observed in the gas phase. The previous *ax* adenine adducts are known to dominate $Rh_2(O_2CCH_3)_4$ chemistry, at least in the early stages of the reactions, owing to favorable hydrogen bond formation between the acetate oxygen atoms and the exocyclic amino group of the adenine.[44−50] Furthermore, the unfavorable binding of guanine to the *ax* positions of $Rh_2(O_2CCH_3)_4$, due to repulsive interactions between the acetate oxygen atoms and the exocyclic ketone O6 of guanine,[48] is likely responsible for the lower percentage of **GG** compared to **AA** adduct signal in the ESI than in the MALDI spectra (Figure 4B). The consequence of the instability of *ax* dirhodium−**GG** adducts is that the bound purine quickly rearranges to *eq* positions to avoid steric repulsions.

For all the dirhodium compounds in this study, the **AG**- and **GA**-containing dodecamers exhibit comparable rates of reactivity with the **AA** and **GG** sequences with the exception of $[Rh_2(O_2CCH_3)_2(CH_3CN)_6]^{2+}$, which is more reactive with the **GG** sequence. Similar rates of reaction between the **AG**- and **GA**-containing sequences have been observed for the first step of formation of monofunctional adducts with activated cisplatin, but a clear preference for the **AG** adduct is observed for cisplatin;[85,95−97] closure of the system ring to form the bifunctional adduct is more rapid for **AG** sequences in both platinum complexes.[98]

The formation of DNA dodecamer dirhodium adducts was found to be independent of the flanking bases (T or C) of the dipurine site in reactions with **GG** dodecamers. The formation of cisplatin 1,2-intrastrand cross links in duplex DNA was also shown to be insensitive to the identity of the flanking pyrimidines of the **GG** site.[93] It is important to point out, however, that cross-linked-induced alterations in the DNA duplex structure, upon metal binding, are modulated by the nature of the base pairs flanking the cross link and are of potential importance for selective recognition of platinated DNA by HMG-domain proteins.[99]

Metal Binding Site Identification. The presence of the $[M + Rh_2(O_2CCH_3)_2 - C_3T_2 - 5H]^{3-}$ ion and the fragmentation adjacent to the **GG** site of the native strand in the CID MS−MS spectrum of [d(CCTCT**GG**TCTCC) + $Rh_2(O_2CCH_3)_2$ − 2H] (Figure 7B) strongly implies that the **GG** residues are the metal binding sites in **GG** dodecamers. The fact that the dirhodium adducts bind to **GG** sites in DNA oligonucleotides was recently established in our laboratories,[58,59,61] a finding that directly contradicts earlier claims that dirhodium guanine adducts are not formed.[37,48]

Enzyme digestion studies followed by MS indicate that the adenine bases are involved in binding for one of the dirhodium bisacetate adducts, [d(CCTTC**AA**CTCTC) + $Rh_2(O_2CCH_3)_2$], isolated by HPLC (Figures 8 and S12 (Supporting Information)). The successive nucleotide cleavage of both enzymes (phopshodieterases I and II) stops at one of the adenine residues, which is an indication that the **AA** bases are the binding sites of the metal.[61,100−102] The fact that the [IV−d(AC_3T_2)] species dominates in the digestions of both enzymes (5′ and 3′) (Figures 8 and S12 (Supporting Information)) further supports this conclusion. The decrease in the intensity of the [(IV)−d(CCTT)] fragment ion and the increase in those of the [(IV)−d(CCTTC)] and [(IV)−d(CCTTCA)] ions as a function of time (Supporting Information, Figure S12B) suggest that the rate of enzyme digestion is slower at the C flanking the A base (perhaps due to conformational changes in the DNA). The increase of the metalated adduct peaks [IV−d(CCTTC)] and [IV−d(CCTTCA)], even after 2 h of enzyme incubation (Supporting Information, Figure S12B), indicates that the rhodium displacement is slow; thus, the **AA** dipurine site is bound to the dirhodium unit. Moreover, the CID MS−MS fragmentation of [d(CCTTC**AA**CTCTC) + $Rh_2(O_2CCH_3)_2$] (Figure 7A), which occurs adjacent to or between the A bases, implies that the DNA backbone is weakened at these sites,[83,103] a finding that corroborates adenine residue binding to the dirhodium core (the dirhodium unit may have been displaced after the fragmentation).

Choice of MALDI versus ESI MS. Owing to the gentle nature of the ESI process,[67] ESI MS proved to be a valuable tool for identifying initial weakly bound dirhodium DNA adducts and for probing possible mechanisms of these reactions. Although MALDI MS is quite useful for monitoring the course of the reactions between oligonucleotides and dirhodium complexes, it cannot be used for the verification of the purity of the adducts due to the high energy of the ionization process, which induces in-source fragmentation (Figure 3). It is important to note, however, that nanoelectrospray mass spectrometry is time consuming and costly; therefore, MALDI is the method of choice for rapid screening of dirhodium−DNA adducts.

Conclusions

An unprecedented comprehensive study of dirhodium−DNA oligonucleotide reactions and identification of their key adducts was carried out by applying MALDI and ESI mass spectrometry coupled with CID techniques, tandem MS

(93) Burstyn, J. N.; Heiger-Bernays, W. J.; Cohen, S. M.; Lippard, S. J. *Nucleic Acids Res.* **2000**, *28*, 4237−4243.
(94) Elmroth, S. K. C.; Lippard, S. J. *Inorg. Chem.* **1995**, *34*, 5234−5243.
(95) Dijt, F. J.; Chottard, J.-C.; Girault, J.-P.; Reedijk, J. *Eur. J. Biochem.* **1989**, *179*, 333−344.
(96) Fouchet, M.-H.; Guittet, E.; Cognet, J. A. H.; Kozelka, J.; Gauthier, C.; Le Bret, M.; Zimmermann, K.; Chottard, J.-C. *J. Biol. Inorg. Chem.* **1997**, *2*, 83−92.
(97) Davies, M. S.; Berners-Price, S. J.; Hambley, T. W. *J. Inorg. Biochem.* **2000**, *79*, 167−172.
(98) Davies, M. S.; Berners-Price, S. J.; Hambley, T. W. *J. Am. Chem. Soc.* **1998**, *120*, 11380−11390.
(99) Pilch, D. S.; Dunham, S. U.; Jamieson, E. R.; Lippard, S. J.; Breslauer, K. J. *J. Mol. Biol.* **2000**, *296*, 803−812.
(100) Cohen, G. L.; Ledner, J. A.; Bauer, W. R.; Ushay, H. M.; Caravana, C.; Lippard, S. J. *J. Am. Chem. Soc.* **1980**, *102*, 2487−2488.
(101) Tullius, T. D.; Lippard, S. J. *J. Am. Chem. Soc.* **1981**, *103*, 4620−4622.
(102) Inagaki, K.; Kasuya, K.; Kidani, Y. *Inorg. Chim. Acta* **1984**, *91*, L13−L15.
(103) Hagemeister, T.; Linscheid, M. *J. Mass Spectrom.* **2002**, *37*, 731−747.

methods, and enzymatic digestion studies. Moreover, a comparison by MALDI of the dirhodium reactivity to the corresponding behavior of platinum compounds with DNA oligonucleotides led to the establishment of the relative reactivity *cis*-$[Pt(NH_3)_2(OH_2)_2]^{2+} \approx Rh_2(O_2CCF_3)_4 >$ *cis*-$[Pt(NH_3)_2Cl_2] \gg [Rh_2(O_2CCH_3)_2(CH_3CN)_6](BF_4)_2 > Rh_2(O_2CCH_3)_4 \approx Pt(C_6H_6O_4)(NH_3)_2$. These results can be rationalized on the basis of lability of the leaving groups, which is one of the determining factors for the outcome of these reactions with DNA. This study indicates that among the dirhodium compounds, $Rh_2(O_2CCF_3)_4$ is the most reactive and would therefore be expected to degrade easily under physiological conditions.

The gentle nature of the electrospray ionization process permitted the observation of initial dirhodium−DNA adducts and intermediates, which contributes to the elucidation of plausible mechanisms for these reactions; the data imply that dirhodium compounds bind to DNA purine sites by establishing weak *ax* interactions followed by rearrangement to more stable *eq* adducts. Enzymatic digestion studies coupled with MALDI and ESI MS studies revealed that, for the dirhodium compounds under consideration, the purine sites of the DNA oligonucleotides interact with the dirhodium core. Both MALDI and ESI MS, when used in a strategic fashion, are complementary, valuable tools for surveying the chemistry of dinuclear metal−DNA adducts and may be successfully applied in the study of other related systems.

Acknowledgment. The LBMS gratefully acknowledges support from NIEHS P30-ES09106, the Robert A. Welch Foundation (A-1176), and the U.S. Department of Energy Division of Chemical Sciences, OBES. K.R.D. thanks Johnson-Matthey for a generous loan of rhodium trichloride and gratefully acknowledges the Welch Foundation (A-1449) and the National Science Foundation (CHE-9906583). J.M.K. gratefully acknowledges stipend support from Ionwerks (NIH SBIR 1R43-GM05773601).

Supporting Information Available: MALDI mass spectra of the reaction mixture of d(CCTCT**GG**TCTCC) with cisplatin, the formation of the platinated oligonucleotide $[M + Pt(NH_3)_2 - 3H]^-$, and the intermediate $[M + Pt(NH_3)_2Cl - 2H]^-$. MALDI mass spectra of reaction mixtures of d(T**GG**T), d(TCT**GG**TCT), and d(CCTCT**GG**TCTCC) with $Rh_2(O_2CCF_3)_4$. ESI mass spectra obtained from reaction mixtures of d(CCTCT**GG**TCTCC) and d(CCTTCC**AA**CTCTC) with $[Rh_2(O_2CCH_3)_2(CH_3CN)_6]^{2+}$ after incubation for 9 days. ESI mass spectra obtained from reaction mixtures of d(TTC**AA**CTC) and d(TCT**GG**TCT) with $Rh_2(O_2CCH_3)_4$. ESI mass spectra obtained from reaction mixtures of d(CCTTC**AA**CTCTC) and d(CCTCT**GG**TCTCC) with $Rh_2(O_2CCH_3)_4$. ESI mass spectra obtained from a reaction mixture of d(CCTCT**GG**TCTCC) with $Rh_2(O_2CCF_3)_4$ at 2.5, 12, and 48 h. MALDI ion signal monitoring the progress of the reactions of $[Rh_2(O_2CCH_3)_2(CH_3CN)_6]^{2+}$, $Rh_2(O_2CCH_3)_4$, and $[Pt(C_6H_6O_4)(NH_3)_2]$ with **AA**, **GG**, **AG**, and **GA** dodecamers. Kinetics of the dodecamer−dirhodium and carboplatin reactions monitored by MALDI for d(CCTTC**AA**CTCTC) and d(CCTCT**GG**TCTCC). MALDI ion signal monitoring the progress of the reactions of $Rh_2(O_2CCF_3)_4$ with **AA**, **GG**, **AG**, and **GA** dodecamers. ESI ion signal monitoring the progress of the reactions of $[Rh_2(O_2CCH_3)_2(CH_3CN)_6]^{2+}$, $Rh_2(O_2CCH_3)_4$, and $[Pt(C_6H_6O_4)(NH_3)_2]$ with the **AA**, **GG**, **AG**, and **GA** dodecamers. In-Source Decay (ISD) fragmentation in MALDI MS of d(CCTTC**AA**CTCTC) adduct with dirhodium bis-acetate. MALDI and ESI MS spectra of the enzymatic digestion products of [d(CCTTC**AA**CTCTC) + $Rh_2(O_2CCH_3)_2$ −2H] (IV) by phosphodiesterase II at 1 and 2.5 h. This material is available free of charge via the Internet at http://pubs.acs.org.

IC040040U